DOE/ET-53088-326 IFSR #326

The Effect of Energetic Trapped Particles on the "Ideal" Internal Kink Mode

Y. Z. Zhang, H. L. Berk, and *S. M. Mahajan*

Institute for Fusion Studies
The University of Texas at Austin
Austin, Texas 78712

December 1988

The Effect of Energetic Trapped Particles on the "Ideal" Internal Kink Mode

Y. Z. ZHANG, H. L. BERK, and S. M. MAHAJAN
Institute for Fusion Studies
The University of Texas at Austin
Austin, Texas 78712

Abstract

The internal kink stability of a tokamak in the presence of energetic particles is studied. It is found that (1) there exists a stable window when a finite population of energetic particles are present, and (2) the relation between the predictions of the fishbone theory of Chen-White-Rosenbluth and the fishbone theory of Coppi-Porcelli is explained. The theory indicates why some experiments, like PDX and TFTR, are likely to see fishbone oscillations in conjunction with sawtooth modes, while other experiments can observe sawtooth suppression in presence of hot particles.

The magnetohydrodynamic (MHD) properties of a tokamak's discharges can be altered due to the kinetic response of the energetic trapped particle component. The effect can be a stabilizing[1] or destabilizing influence especially on the internal kink. Experimentally, the destabilizing influence has been observed in fishbone oscillations of neutral beam injected plasmas,[4–6] while the stabilizing behavior has been observed in JET[7,8] in ICRF heated plasmas with an energetic minority ion component.

The theories have been developed by several authors[2,3,9–11] for the internal kink with finite ω_i^* (the background ion diamagnetic frequency) under the influence of energetic ions in an effort to explain both the fishbone and the stabilization of the MHD behavior. We describe an analysis of Coppi-Porcelli dispersion relation.[3] It is obtained by treating the kink layer in the ideal MHD limit with the correction due to finite ω_i^* (henceforth, it is referred to be "zero" FLR theory). Modifications in the results are expected from large ion Larmor radius and finite conductivity effects within the layer.[12,13] These effects will be reported in subsequent work. In this letter we only present the results from the "zero" FLR theory, and stress the relationship between the earlier contending theories of fishbone oscillations.[2,3]

The dispersion relation of the "zero" FLR theory is[3]

$$\omega_A \delta\hat{W} - i\sqrt{\omega\left(\omega - \omega_i^*\right)} = 0, \tag{1}$$

where ω_A is the Alfvén frequency, $\delta\hat{W} = \delta\hat{W}_c + \delta\hat{W}_h$. $\delta\hat{W}_c$ is the normalized MHD energy of background plasma. We shall use the specific $\delta\hat{W}_c$ obtained by Bussac[14]

$$\delta\hat{W}_c \;=\; 3\left(1 - q(0)\right)\left(\frac{13}{144} - \tilde{\beta}_p^2\right)\left(\frac{r_s}{R}\right)^2 \tag{2}$$

with

$$\tilde{\beta}_p \;=\; -\left(\frac{8\pi}{B_p^2}\right)\int_0^{r_s/a} dx\, x^2 \left(\frac{dP}{dx}\right), \tag{3}$$

where B_p is the poloidal field at the $q = 1$ surface, p is the background plasma pressure, r_s is the position of the $q = 1$ surface, a and R the minor and the major radius, respectively, $q(0)$

the safety factor at $x \equiv r/a = 0$. $\delta\hat{W}_h$ is the hot particle energy with the same normalization as the above to δW_h with

$$\delta W_h \sim -\frac{1}{2}\int d^3r\,|\xi_r|^2\,\omega\left(\frac{e_h B r}{c}\right)\int d\Gamma \frac{\omega_{dh}}{\omega-\bar{\omega}_{dh}}\cdot\frac{\partial F_h}{\partial r}, \tag{4}$$

where e_h is the hot particle charge (always positive in this letter), ω_{dh} and $\bar{\omega}_{dh}$ are the hot particle drift frequency and its line average, respectively, $d\Gamma$ is the velocity-space volume element, F_h is the equilibrium distribution of the hot particles, and ξ_r is the radial component of the plasma displacement. For simplicity, we choose a slowing down energy distribution with a δ-function in the pitch angle to obtain

$$\delta\hat{W}_h \;=\; \tilde{\beta}_h\hat{\omega}\ln\left(1-\frac{1}{\hat{\omega}}\right), \tag{5}$$

with

$$\tilde{\beta}_h \;=\; -\left(\frac{R}{3a}\right)I\left(\kappa_0^2\right)a\frac{\partial\left\langle\beta_h\right\rangle_\theta}{\partial r}, \tag{6}$$

where R/a is the aspect ratio, $\langle\beta_h\rangle_\theta$ is the poloidally averaged β_h, the hot particle β-value, $I\left(\kappa_0^2\right) = 2E\left(\kappa_0^2\right)/K\left(\kappa_0^2\right) - 1. \sim 1-\kappa_0^2$ for deeply trapped particles comes from the line average of $\cos\theta$ (characteristic of the normal curvature), E and K are the complete elliptic integrals, $\kappa_0^2 = \kappa^2\left(\alpha_0\right)$ with $\kappa^2(\alpha) \equiv (R/2r)(1/\alpha - 1 + r/R)$ and $\hat{\omega} = \omega/\bar{\omega}_{d0}$ is the normalized frequency with $\bar{\omega}_{d0} = (c/eBr_sR)\,I\left(\kappa_0^2\right)E_{\max}$, denoting the line average drift frequency of the trapped hot particles, $E_{\max}$ is the maximum energy, evaluated at $\kappa^2 = \kappa_0^2$, $r = r_s$.

We now analyze the dispersion relation, Eq. (1), with $\omega_i^* = 0$.

$$-\Lambda + \hat{\beta}_h\hat{\omega}\ln\left(1-\frac{1}{\hat{\omega}}\right) - i\hat{\omega} = 0, \tag{7}$$

where $\Lambda = -\delta\hat{W}_c\hat{\omega}_A$ and $\hat{\beta}_h = \tilde{\beta}_h\hat{\omega}_A$, $\hat{\omega}_A = \omega_A/\bar{\omega}_{d0}$. We solve Eq. (7), both analytically and numerically. The numerical results will be presented first. In Fig. 1, we plot the loci of the $\mathrm{Re}\,\hat{\omega}$ versus $\mathrm{Im}\,\hat{\omega}$ curves as $\hat{\beta}_h$ varies. Each curve is for a fixed value of Λ, and we have chosen to display curves with $\Lambda = 0.0,\ 0.05,\ 0.08,\ 0.09$. The $\hat{\beta}_h$ values are indicated by the

darkened points on the plot. Notice that the nature of the curve changes fundamentally as Λ crosses the critical value of $\Lambda_c = 0.0866$. For $\Lambda < \Lambda_c$ there are two unstable branches, a low-frequency branch (the MHD mode) and a high-frequency branch (the precessional mode). As $\hat{\beta}_h$ increases, the MHD mode is first destabilized, but then its growth rate decreases reaching marginal stability at $\hat{\beta}_h = 1/\pi$. However, the $\hat{\beta}_h = 1/\pi$ value is precisely the onset of the precessional mode growth, which eventually becomes larger than the real frequency.

For $\Lambda > \Lambda_c = 0.0866$, however, large $\hat{\beta}_h$ can no longer completely stabilize the MHD mode (curve d in Fig. 1). Instead, the nature of the unstable mode gradually changes from the MHD mode to the precessional mode, without marginal stability ever arising.

These numerical results can be understood analytically as follows. From Eq. (7) we observe that without hot particles, we have a purely growing MHD mode, $\hat{\omega} = i\Lambda$. For very small values of $\hat{\beta}_h$, the mode frequency can be perturbatively calculated. For $\hat{\beta}_h > 0$ the growth rate shows a small increase and the mode also acquires a small real frequency

$$\hat{\omega} \sim i\Lambda \left[1 + \hat{\beta}_h \tan^{-1}\left(\frac{1}{\Lambda}\right)\right] + \frac{1}{2}\hat{\beta}_h \Lambda \ln\left(1 + \frac{1}{\Lambda}\right) + O\left(\hat{\beta}_h^2\right). \tag{8}$$

This character of $\hat{\omega}$ is observed in the $\mathrm{Re}\,\hat{\omega} \simeq 0$ part of Fig. 1, where we also see that negative $\hat{\beta}_h$ is always stabilizing. For $\hat{\beta}_h > 0$ Fig. 1 indicates that the growth rate peaks and then decreases. But stability of the MHD mode only arises if $\Lambda < \Lambda_c$. To calculate Λ_c we set to zero the real and imaginary part of Eq. (7), assuming $0 < \hat{\omega} < 1$. As marginal stability ($\mathrm{Im}\,\hat{\omega} = 0$), we obtain $\hat{\beta}_h = 1/\pi$, and

$$\Lambda = \frac{\hat{\omega}_r}{\pi} \ln\left|1 - \frac{1}{\hat{\omega}_r}\right| \equiv f\left(\hat{\omega}_r\right), \tag{9}$$

which must have a solution for marginal stability to be accessible. The function $f(\hat{\omega})$ has a maximum at $\hat{\omega}_0 = 0.2178\ldots$, where $f\left(\hat{\omega}_0\right) = 0.08863\ldots \equiv \Lambda_c$. Thus, when $\hat{\beta}_h = 1/\pi$ and $\Lambda < \Lambda_c$, Eq. (9) has real solutions; there are two marginal stable roots, a low-frequency root for which $\hat{\omega} < \hat{\omega}_0$ (the MHD mode) and a high-frequency root, for which $\omega > \omega_0$ (the precessional mode, its destabilization is precisely the fishbone mode referred by Chen,

White, and Rosenbluth[2]). Straightforward analysis indicates that the precessional wave is destabilized for $\hat{\beta}_h > 1/\pi$, as observed in Fig. 1. Thus, for any value of $\hat{\beta}_h$ there is an unstable mode. We note that this dramatic property depends on the approximations used in the calculations of $\delta\hat{W}_h$, in particular on the specific distribution that has been chosen in which the pole contributions to δW_h [Eq. (4)] is only linearly dependent on ω. If $\Lambda > \Lambda_c$ there is no solution to Eq. (9), and hence no stabilization; the MHD mode blends into the precessional mode as $\hat{\beta}_h$ increases.

We now investigate the effects of finite ω_i^* on the results presented in Fig. 1. An exact analytic solution can be obtained for the marginal stability of the precessional mode if $\Lambda = 0$. The vanishing of the real part of the dispersion relation demands $\hat{\omega} = 0.5$. Substituting this $\hat{\omega}$ into the imaginary part of the dispersion relation yields

$$\hat{\beta}_h = \hat{\beta}_h^{(0)} \equiv \frac{\sqrt{1-2\hat{\omega}_i^*}}{\pi}. \tag{10}$$

For finite but small Λ $\left(\Lambda/\hat{\beta}_h^{(0)} \ll 1\right)$ the dispersion relation yields

$$\hat{\omega} = \frac{\left(1-\Lambda/\hat{\beta}_h^{(0)}\right)}{2}$$

and the conditions for marginal stability becomes

$$\hat{\beta}_h = \frac{\sqrt{1-2\hat{\omega}_i^*/\left(1-\Lambda/\hat{\beta}_h^{(0)}\right)}}{\pi}. \tag{11}$$

We now turn our attention to the discussion of the MHD mode with corrections due to ω_i^*. In the absence of hot particles, the MHD modes are determined by solving $\Lambda + i\sqrt{\omega\left(\omega-\omega_i^*\right)} = 0$, giving two marginal stable modes[3] for $\hat{\omega}_i^* > 2\Lambda$ with frequencies

$$\hat{\omega} = \frac{\hat{\omega}_i^*}{2} \pm \frac{1}{2}\sqrt{\hat{\omega}_i^{*2} - 4\Lambda^2}.$$

The high-frequency mode will be referred to as the ω_i^* mode and its destabilization is precisely the fishbone mode referred by Coppi and Porelli.[3] The other mode will be referred to as the low-frequency mode. Assuming the real frequency of the ω_i^* mode to be less than $\bar{\omega}_{d0}$ $(\hat{\omega}_i^* < 1)$,

one observes that the dissipation, introduced by a small $\hat{\beta}_h$ term, destabilizes one of the real frequency modes; if $\hat{\beta}_h > 0$, the ω_i^* mode is destabilized, while if $\hat{\beta}_h < 0$, the low-frequency mode is destabilized. To obtain marginal stability with ω_i^* and $\hat{\beta}_h$ we analyze the real and imaginary parts of Eq. (7). From the imaginary part we find $\hat{\omega} = \hat{\omega}_i^* / \left(1 - \pi^2 \hat{\beta}_h^2\right)$. If we assume $\pi \hat{\beta}_h \ll 1$, the marginal stability condition for the ω_i^* mode becomes

$$\hat{\beta}_h = \frac{\Lambda}{\hat{\omega}_i^* \ln\left(1/\hat{\omega}_i^* - 1\right)}. \tag{12}$$

Note that in achieving the stability condition the real part of ω has changed from $\omega < \omega_i^*$ (for low $\hat{\beta}_h$) to $\omega > \omega_i^*$. Equation (12) also indicates that the threshold depends primarily on the density of the hot species; the temperature dependence arising only from the logarithm term. However, an important hot particle temperature threshold arises from the condition that the argument of the logarithm is bigger than unity leading to $\hat{\omega}_i^* \lesssim 1/2$. As $\hat{\omega}_i^* \sim 1/E_{\max}$, we see that there is a threshold for hot particle energy to achieve stabilization.

To understand the interaction between the precessional mode and the ω_i^* mode, we must again resort to numerical work. In Fig. 2a and 2b, we display the numerical solution of the dispersion relation plotting $\mathrm{Re}\,\hat{\omega}$ and $\mathrm{Im}\,\hat{\omega}$ as function of $\hat{\beta}_h$. These figures illustrates the effect of finite ω_i^* on the various modes present. For $\Lambda = 0.05$, we present two sets of curves for $\hat{\omega}_i^* = 0$ and $\hat{\omega}_i^* = 0.2$, respectively. The behavior of the $\hat{\omega}_i^* = 0$ curves has already been discussed (this example corresponds to $\Lambda < \Lambda_c$). We had found earlier that $\hat{\omega}_i^*$ ($\hat{\omega}_i^* < 0.5$) tends to destabilize the precessional mode [c.f. Eqs. (10), (11)]. We also know that the low-frequency mode (without the hot particles) are marginally stable for $\hat{\omega}_i^* > 2\Lambda$. Our choice of $\hat{\omega}_i^* = 0.2$, $\Lambda = 0.05$ does satisfy this inequality. As a result of these opposing effects of ω_i^*, it turns out in the presence of hot particles the dispersion relation allows a stability window, i.e., there exists a range of $\hat{\beta}_h$, in which neither of the branches is unstable. This behavior is illustrated by the dashed lines of Fig. 2b, and is to be contrasted with $\hat{\omega}_i^* = 0$ case (represented by solid and solid-dot lines), where for all values of $\hat{\beta}_h$, there exists an unstable mode.

Since the existence of a stability window is crucial to the understanding of the system, we draw the marginal stability contours in the $\hat{\beta}_h - \hat{\omega}_i^*$ plane (Fig. 3a). These two parameters along with Λ are the determining parameters of the system behavior. We have chosen to display curves with $\Lambda = 0.0,\ 0.01,\ 0.03,\ 0.05$. As Λ increase, the stable regions are getting smaller, and vanish when $\Lambda = \Lambda_c \sim 0.09$. Making use of Bussac formula for $\delta\hat{W}_c$, Eq. (2), we estimate the maximum $\tilde{\beta}_p$ [defined by $\Lambda = \Lambda_c$ and Eqs. (2)–(3)] can be three times of the critical $\tilde{\beta}_p(\sim 0.3)$ for currently operating tokamaks. The upper edges of the stability boundaries correspond to the precessional mode, and the lower edges to the ω_i^* mode. However, when ω_i^* is raised, these two modes are converted to each other, which can be clearly seen in Fig. 3b for the real frequencies at the marginal stability.

We now assess the stability of the low-frequency mode when $\hat{\beta}_h$ is negative within the $q = 1$ surface. The negative $\hat{\beta}_h$ implies a stable precessional mode. For $\Lambda > 0$ and $\omega_i^* > 2\Lambda$ the low-frequency mode with the mode frequency $\hat{\omega}_0 \sim \Lambda^2/\hat{\omega}_i^*$ is destabilized by this negative $\hat{\beta}_h$. We note that electron dissipation has not been included in this analyses and is expected to help stabilize this mode. One further problem is the low-frequency nature of this mode force a break-up of a basic assumption in the derivation of the dispersion relation, viz. the mode frequency larger than the grad-B frequency of the background plasma. Thus a more complicated theory including ion drift effects and electron dissipation is needed to describe stability, a problem that is beyond the scope of this letter.

Finally, to elucidate the experimental significance of the present theory, two tables are given below, showing the relationship between experiments and theory. Since big uncertainties exist for estimate of $\delta\hat{W}_c$ and $\tilde{\beta}_h$, we simply claim $\delta\hat{W}_c \sim -1 \times 10^{-3}$ and $\hat{\beta}_h \sim 0.15 \pm 0.15$. However, we still may conclude that the fishbone oscillations in PDX and TFTR are likely caused by too high $\hat{\omega}_i^*$ value, while the operation in JET and Doublet-III may or may not be stable, depending on the $\hat{\beta}_h$ and $\delta\hat{W}_c$ values. We must point out that the serious comparison between the theory and experiments should be given on the basis of a more sophisticated

theory, which includes the effects due to arbitrary Larmor radius and finite conductivity within the layer. However, we expect that even when these effects are included, there will not be any stable window for $\hat{\omega}_i^* \gtrsim 0.5$, as shown by our current work.[12] Therefore, it appears that the fishbone oscillations observed in PDX and TFTR arises in a parameter regime where the precessional mode (Chen-White-Rosenbluth fishbone[2]) and the ω_i^* mode (Coppi-Porcelli fishbone[3]) merge. In other machines such as JET and Doublet-III the ω_i^* value are such to exhibit a separation of the ω_i^* and precessional modes, as well as provide a stable window of operation.

Acknowledgements

We would like to acknowledge helpful discussions with Dr. James Van Dam. This work was supported by U. S. Dept. of Energy Contract No. DE-FG05-80ET-53088.

References

1. M. N. Rosenbluth, S. T. Tsai, J. W. Van Dam, and M. G. Engquist, Phys. Rev. Lett. **51**, 1967 (1983).

2. L. Chen, R. B. White, and M. N. Rosenbluth, Phys. Rev. Lett. **52**, 1122 (1984).

3. B. Coppi and F. Porcelli, Phys. Rev. Lett. **57**, 2272 (1986).

4. PDX Group, Phys. Rev. Lett. **50**, 891 (1983).

5. Doublet-III Group, Heating in Toroidal Plasmas 1984, edited by H. Knoepfel and E. Sindoni, ENEA (Rome), Vol. I, p. 21 (1984).

6. R. Kaita, R. B. White, A. W. Morris, E. D. Fredrickson, K. M. McGuire, S. S. Medley, and S. D. Scott, Princeton Plasma Physics Laboratory Report PPPL-2493 (January 1988).

7. J. Jacquinot, et al., Eleventh International Conference on Plasma Physics and Controlled Nuclear Fusion Research (Kyoto, Japan), (IAEA, Vienna, 1987) Vol. I, p. 449.

8. D. J. Campbell, et al., Twelfth International Conference on Plasma Physics and Controlled Nuclear Fusion Research (Nice, France), IAEA-CN-50/A-7-2 (1988).

9. R. B. White, M. N. Bussac, and F. Romanelli, Princeton Plasma Physics Laboratory Report PPPL-2540 (1988).

10. B. Coppi, R. J. Hastie, S. Migliuolo, F. Pegraro, and F. Porcelli, Phys. Lett. **A132**, 267 (1988); and F. Pegoraro, F. Porcelli, B. Coppi, P. Detragiache, and S. Migliuolo, Twelfth International Conference on Plasma Physics and Controlled Nuclear Fusion Research (Nice, France), IAEA-CN-50/D-4-6 (1988).

11. G. Y. Fu, J. W. Van Dam, M. N. Rosenbluth, D. W. Ross, Y. Z. Zhang, H. L. Berk, S. M. Mahajan, C. Z. Cheng, R. L. Miller, X. H. Wang, A. Bhattacharjee, M. E. Mauel, and B. Breizman, Twelfth International Conference on Plasma Physics and Controlled Nuclear Fusion Research (Nice, France), IAEA-CN-50/D-4-11 (1988).

12. Y. Z. Zhang, Bull. Am. Phys. Soc. **33**, 2074 (1988).

13. F. Pegoraro, F. Porcelli, and T. J. Schep, submitted to Phys. Fluids.

14. M. N. Bussac, R. Pellat, D. Edery, and J. L. Soule, Phys. Rev. Lett. **35**, 1638 (1975).

Table I. The estimate of parameters in the theory for tokamaks.[a]

	PDX	Doublet-III	TFTR	JET
$\hat{\omega}_i^*$	0.4	0.1	0.8	4×10^{-2}
$\hat{\omega}_A$	3.8	3.9	35	4.0
$-\delta\hat{W}_c\hat{\omega}_A$	3.8×10^{-3}	3.9×10^{-3}	3.5×10^{-2}	4×10^{-3}

[a]We use ad hoc estimates for $\delta\hat{W}_c \sim -1 \times 10^{-3}$, and for the shear $\hat{s} \equiv r_s(dq/dr) \sim 0.5$. Other parameters for estimate of $\hat{\omega}_i^*$ and $\hat{\omega}_A$ are given in Table II.

Table II. The typical parameters for tokamaks.[b]

	PDX	Doublet-III	TFTR	JET
$B_{[T]}$	1.1	1.3	3.0	2.1
$n\,[10^{13}\mathrm{cm}^{-3}]$	6.6	5.3	3.5	3.0
T_i[kev]	2.0	1.3	13.4	5.0
R[m]	1.4	1.4	2.5	3.0
r_s[m]	0.2	0.2	0.35	0.4
E_h[kev]	50	75	95	~ 500
L_p[m]	0.2	0.6	0.8	1.2

[b]The parameters given here in PDX, TFTR, and Doublet-III are those in fishbone regime. The parameters in JET are those in sawtooth stabilization regime.

Figure Captions

1. The locus of solution of the ideal MHD mode under the influence of energetic trapped particles with $\omega_i^* = 0$ in the complex plane as a function of $\hat{\beta}_h \equiv \tilde{\beta}_h \hat{\omega}_A$. Curves a, b, c, d stand for $\delta\hat{W}_c\hat{\omega}_A = 0.0, -0.05, -0.08, -0.09$, respectively. The dashed curve stands for $\delta\hat{W}_c\hat{\omega}_A = -0.0866$.

2. The real frequencies (Fig. 2a) and growth rate (Fig. 2b) versus $\hat{\beta}_h \equiv \tilde{\beta}_h\hat{\omega}_A$ of ideal modes for illustration of mode conversion between the precessional mode and the MHD mode. The solid lines and dot-dash lines represent $\hat{\omega}_i^* = 0$, $\delta\hat{W}_c\hat{\omega}_A = -0.1, -0.05$, respectively. The dashed lines represent $\hat{\omega}_i^* = 0.2$, $\delta\hat{W}_c\hat{\omega}_A = -0.05$.

3. (a) The stability boundaries of Eq. (1) on $\hat{\beta}_h - \hat{\omega}_i^*$ plane $\left(\hat{\beta}_h \equiv \tilde{\beta}_h\hat{\omega}_A\right)$ with $\delta\hat{W}_c\hat{\omega}_A = 0.0, -0.01, -0.03, -0.05$, respectively. The stable region is the area enclosed by the corresponding curve.

   (b) The real frequencies at the marginal stability versus $\hat{\omega}_i^*$ with the same $\delta\hat{W}_c\hat{\omega}_A$ in curves a, b, c, d as in Fig. 3a. The corresponding $\hat{\beta}_h$ can be found from Fig. 3a by using the same $\hat{\omega}_i^*$-value.

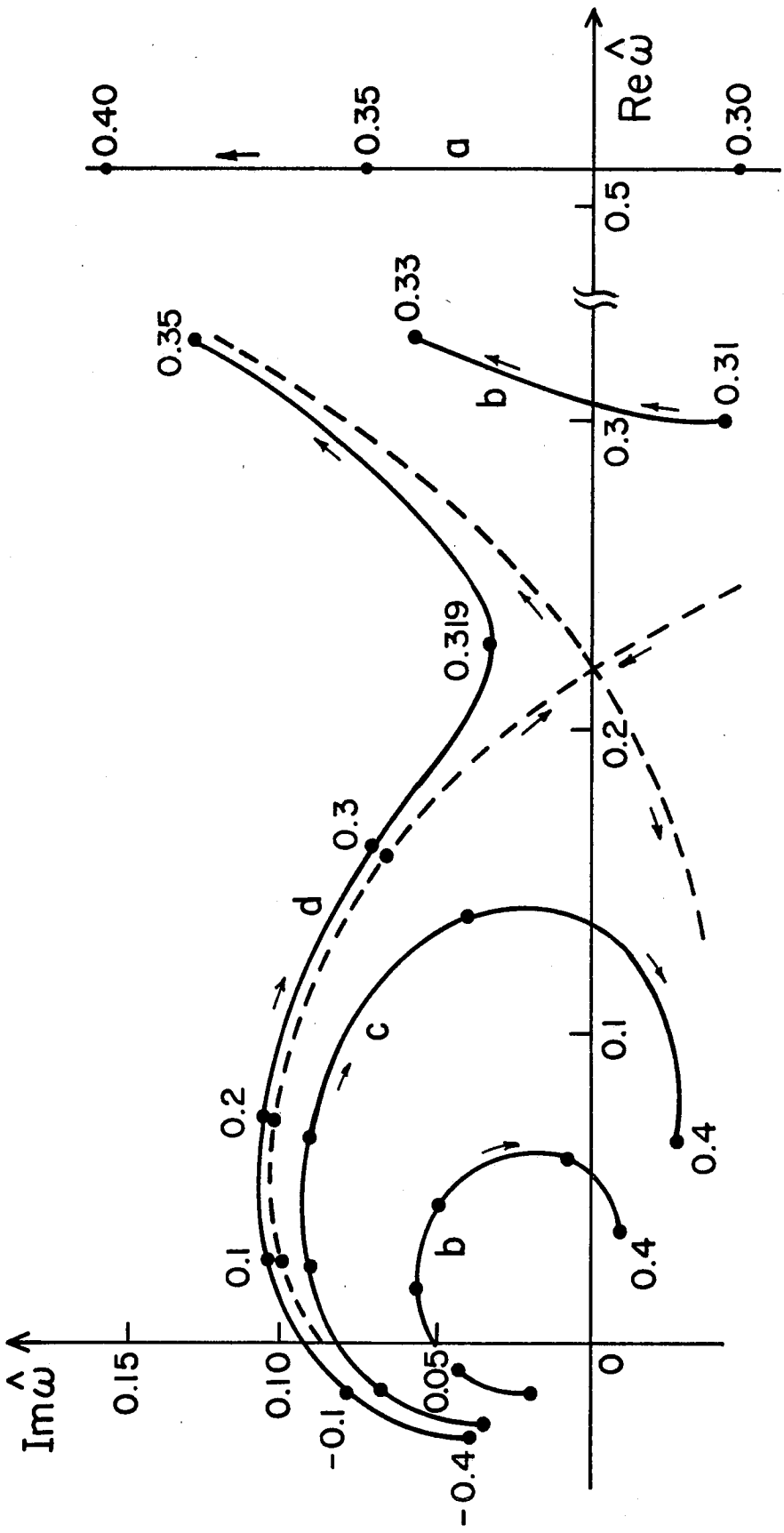
Re ω̂
0.40
0.35
0.30
a
0.5
0.33
0.31
b
0.3
0.35
0.319
0.2
0.3
d
c
0.1
0.2
0.4
0.1
b
0.4
Im ω̂
0.15
0.10
0.05
0
-0.1
-0.4

Figure 1

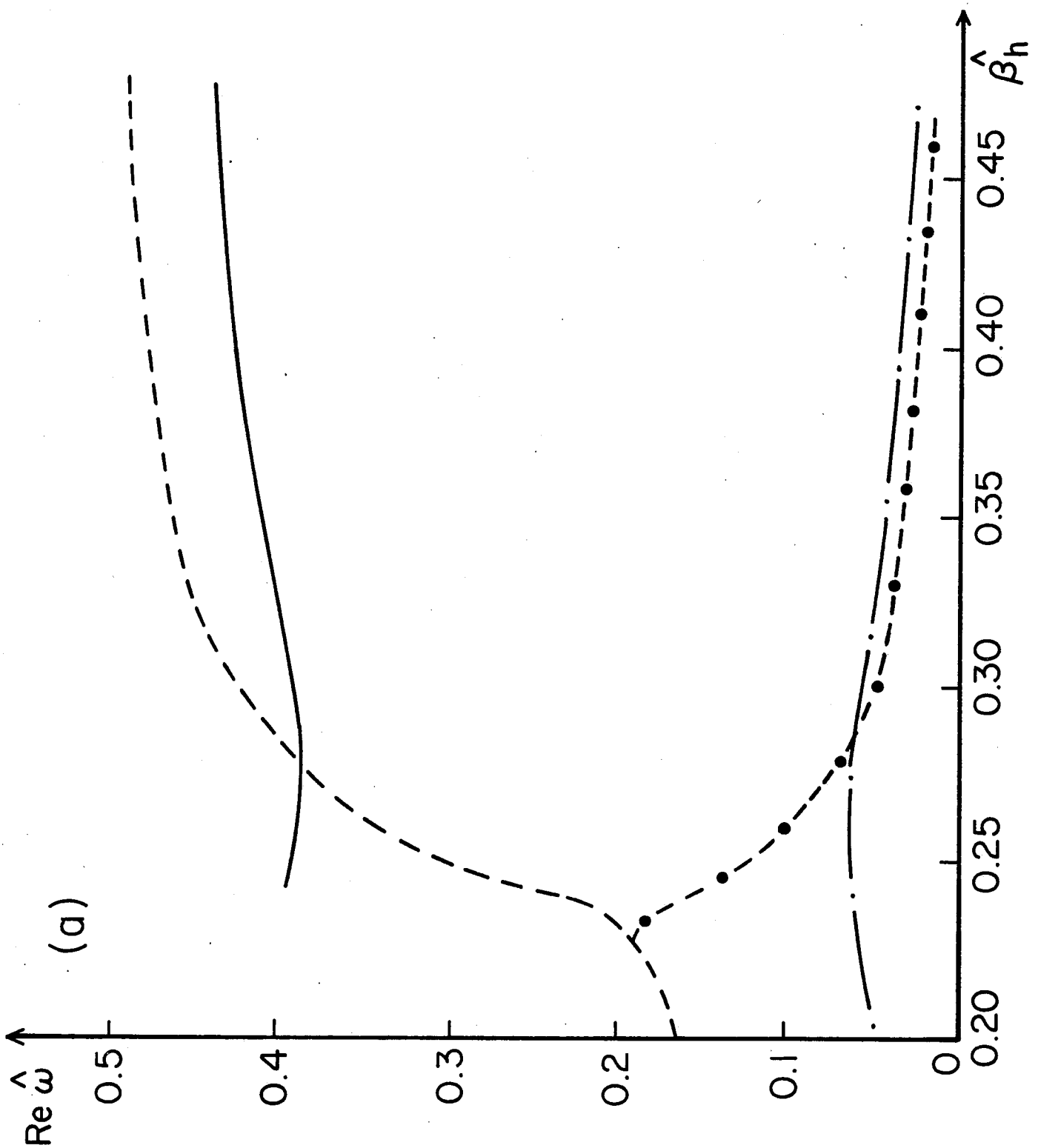

Figure 2a

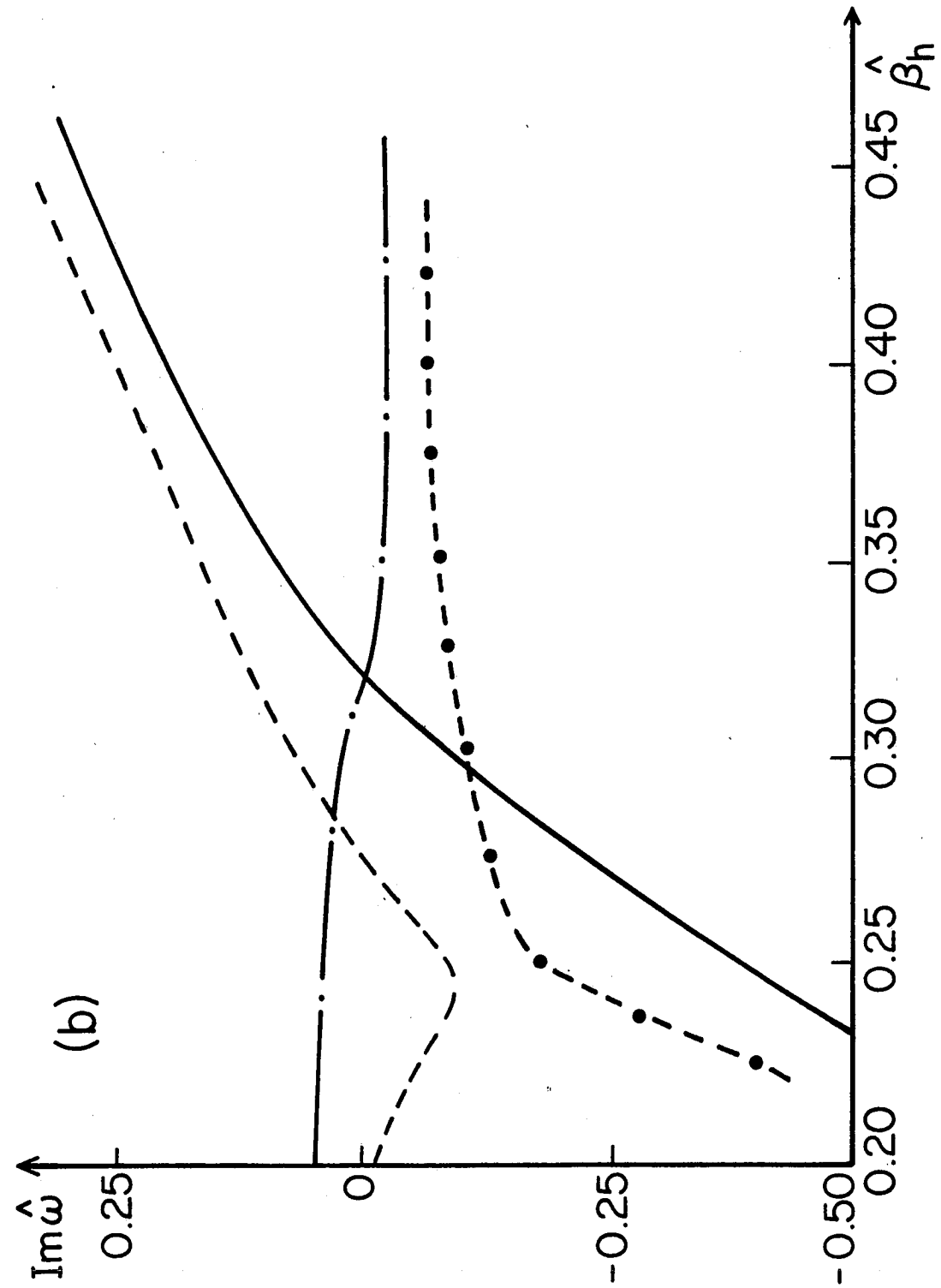

Figure 2b

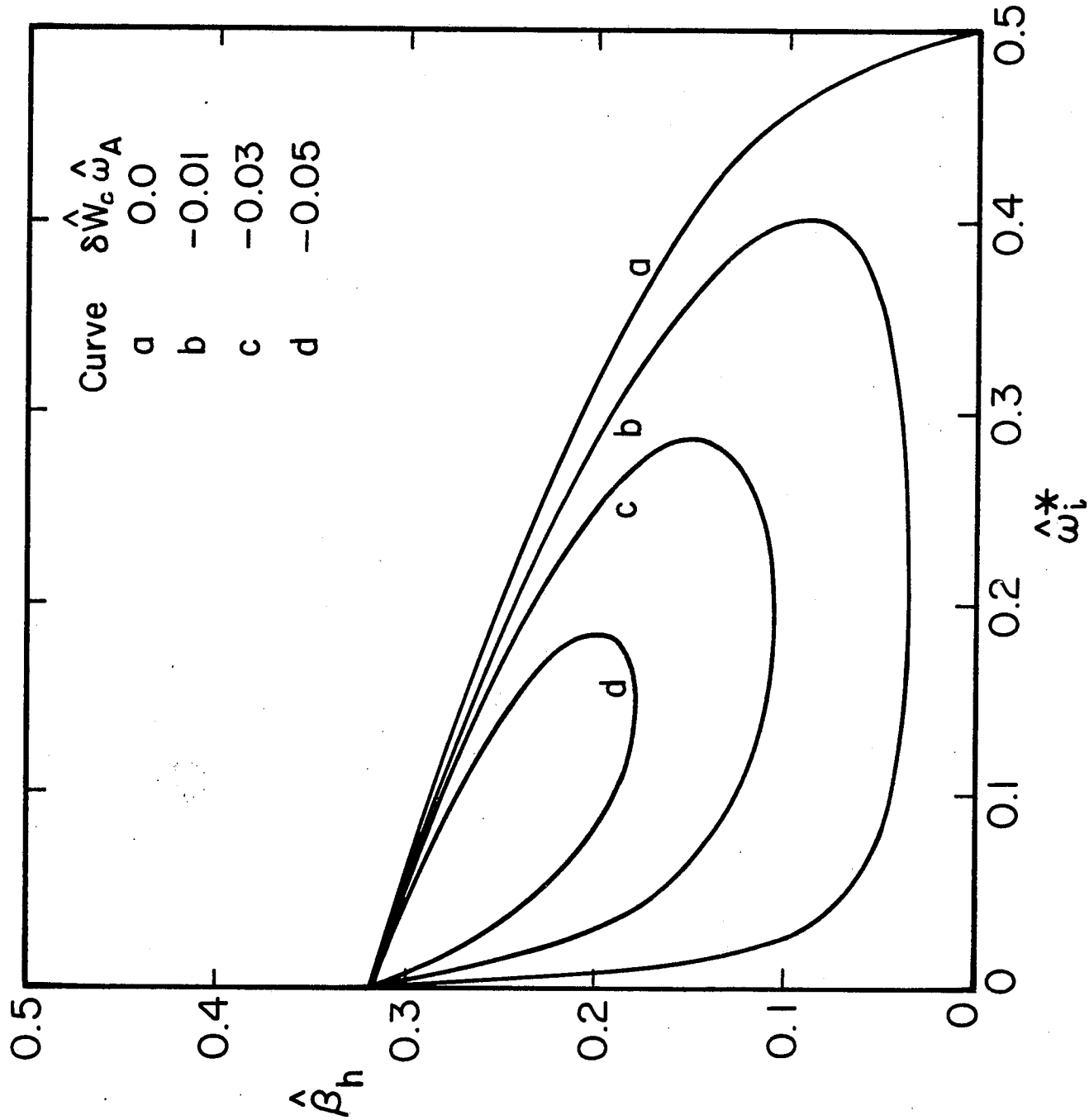
Curve $\delta\hat{W}_c$ $\hat{\omega}_A$
a 0.0
b −0.01
c −0.03
d −0.05
a
b
c
d
0.5
0.4
0.3
0.2
0.1
0
$\hat{\beta}_h$
$\hat{\omega}_i^*$

Figure 3a

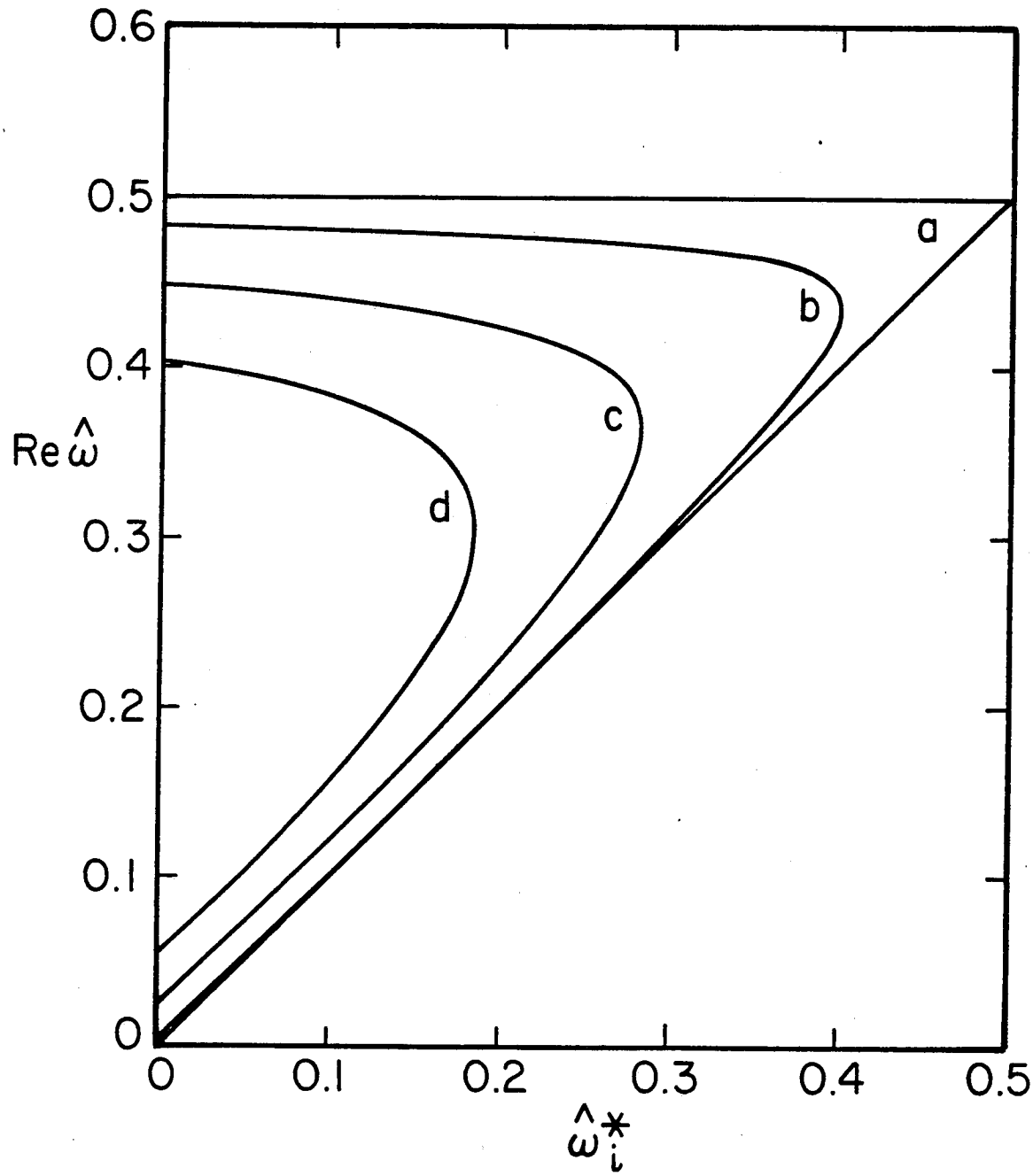

Figure 3b